Article

The role of synoptic cyclones for the formation of Arctic summer circulation patterns as clustered by self-organizing maps

Min-Hee Lee [1] and Joo-Hong Kim [1,*]

[1] Korea Polar Research Institute, 26, Songdomirae-ro, Yeonsu-gu, Incheon 21990, Korea; mhlee@kopri.re.kr
* Correspondence: joo-hong.kim@kopri.re.kr

Abstract: The contribution of extra-tropical synoptic cyclones to the formation of summer-mean atmospheric circulation patterns in the Arctic is investigated by clustering the dominant Arctic circulation patterns by the self-organizing maps (SOMs) using the daily mean sea level pressure (MSLP) in the Arctic domain (≥ 60°N). Three SOM patterns are identified: one with prevalent low pressure anomalies in the Arctic Circle (SOM1) and two opposite dipoles with primary high pressure anomalies covering the Arctic Ocean (SOM2 and SOM3). The time series of summertime occurrence frequencies demonstrate the largest inter-annual variation in the SOM1, the slight decreasing trend in the SOM2, and the abrupt upswing after 2007 in the SOM3. The relevant analyses with produced cyclone track data confirm that the vital contribution. The Arctic cyclone activity is enhanced in the SOM1 because the meridional temperature gradient increases over the land–Arctic Ocean boundaries co-located with major cyclone pathways. The composite daily synoptic evolutions for each SOM reveal that the persistence of all the three SOMs is less than 5 days on average. These evolutionary short-term weather patterns have substantial variability at inter-annual and longer timescales. Therefore, the synoptic-scale activity is central to forming the seasonal-mean climate of the Arctic.

Keywords: Arctic summer circulation patterns, Extra-tropical synoptic cyclones, Self-organizing maps (SOMs), Cyclone detection and tracking

1. Introduction

Low-frequency atmospheric circulation modes in the Arctic (e.g., the Arctic Oscillation (AO), Dipole Anomaly (DA), etc.) have been of high interest as a controlling factor of the spatio-temporal sea-ice variability [1–3], as it could have been investigated in various methods through relatively more abundant atmospheric data sources, compared with the ocean circulation pattern. Among seasons, the summer circulation pattern has been paid attention as its temporal proximity to the September sea-ice minimum [4–9]. However, earlier preconditioning factors during previous winter and spring have been also attracted much attention due to their value for long-lead seasonal prediction [10–12].

The summer season is known to be the most synoptically active in the Arctic Ocean [13–15]. As high-latitude sea-ice and snow gradually disappear by seasonal warming, the meridional thermal contrast between the land and ocean preferentially forms the baroclinic frontal zone along the land-ocean boundary [16]. As a result, the summer in the Arctic Ocean is stormier than the winter, by local cyclogenesis, as well as by migratory mid-latitude cyclones [14]. Therefore, the Arctic cyclone itself and its role in controlling sea-ice have been critical topics to understand the Arctic summer [17–19].

In a scale interaction perspective, the Arctic is a singular region where the zonal scales from synoptic to planetary merge, due to reduced length of latitudinal circles. If a strong synoptic cyclone/anticyclone persists or synoptic cyclones/anticyclones frequently pass near the pole, it can

directly contribute to the low-frequency (i.e., monthly-to-seasonal) large-scale circulation pattern therein [13,14,20]. [14] showed that the cyclone activity is dominant during the cyclonic summer sea level pressure pattern through the composite analysis and case investigation. On the other hand, [20] revealed that the episodic synoptic anticyclones in the Arctic favor anticyclonic summer seasonal circulation that accounts for more summer sea-ice melting.

As described above, previous studies suggested that the accumulation of synoptic events is relevant for generating a preferred pattern of seasonal circulation in the Arctic, but none of them tried to investigate the quantitative contribution of synoptic cyclones to individual summer-mean large-scale circulation patterns in the Arctic. Accordingly, the detection and tracking of extra-tropical synoptic cyclones are carried out to quantify cyclone activity and relate it with the summer-mean Arctic circulation patterns. We also need to identify the summer-mean Arctic circulation patterns with a relevant pattern classification method. Among methods, we adopt the self-organizing maps (SOMs) which has been proven to effectively distinguish the representative patterns from the large climate data set [21–24]). [21] have identified the continuum of El Niño–Southern Oscillation (ENSO)-related sea surface patterns. [22] have used for distinguishing the shift of atmospheric jet that are not separated by empirical orthogonal functions (EOFs). In addition, the SOMs have been used to distinguish the patterns related to the variabilities of the winter cold extremes over North America and Europe [23] and the summer hot extremes over the Northern Hemisphere [24]. These studies have concluded that the clusters derived from the SOMs are more accurate and linearly independent than those from commonly used hierarchical cluster analysis.

This study is structured as follows. Section 2 provides the descriptions of the data and analysis methods including the SOM clustering, detection and tracking of synoptic cyclones and grid-cell representation of cyclone activity. Section 3 presents the representative SOM patterns of Arctic large-scale surface circulation during summer and their inter-annual variations. Furthermore, associated with individual SOM patterns, this section also shows the synoptic cyclone activities, the analyses relevant to the cyclone development and the daily synoptic evolution of large-scale circulation in the Arctic. Finally, summary and discussions are given in Section 4.

2. Data and Methods

2.1. Data

This study primarily used the atmospheric fields of the European Centre for Medium-Range Weather Forecasts Interim Reanalysis (ERA-Interim) dataset [25] with the 1.5°×1.5° horizontal resolution during boreal summer (June-July-August, JJA) of 1979–2017. The SOM clustering algorithm utilized the daily mean sea level pressure (MSLP) field with its climatological-mean of 1-2-1 smoothed daily seasonal cycle being removed. The further atmospheric analyses corresponding to SOM clusters were carried out with the horizontal winds, temperatures, and geopotential heights between 850 hPa and 200 hPa. For storm detection, the 6-hourly fields of the MSLP and 850-hPa relative vorticity were used as the input for the storm detection algorithm used (see Section 2.3).

2.2. Self-organizing maps (SOMs)

The SOM algorithm is one of the clustering methods, which originates form neural networks (refer to the appendix in [26] for more details). Because it is based on the K-means clustering, it classifies data into a specified number of clusters through supervised machine learning. It differs from the other clustering methods in that it relocates the resultant clustering patterns onto a one- or two-dimensional grid based on the pattern similarity between clusters [27]. This ad-hoc relocation enables us to describe a continuum of atmospheric circulation regimes [21,26,28].

During the training period, individual data are partitioned into a particular SOM pattern to which the Euclidean distance from the data is minimum. Here it means that each daily MSLP pattern should have its best-matching SOM pattern. Naturally the two patterns match better as the predefined number of SOM patterns increases, but too large numbers of SOM clusters are less useful for clearly identifying the different physical modes in the data. Therefore, it is generally

recommended to determine the optimal number of SOM patterns by satisfying the following two conditions; (1) the number of SOM patterns is large enough to accurately capture the physical characteristics of the data, and, at the same time, (2) it needs to be sufficiently small so that the clusters are distinctive from each other. To find the optimal number of SOM patterns satisfying the both conditions, we compute (1) the average pattern correlations between the daily fields and their best-matching SOM pattern [22] and (2) the distance between different cluster pairs (d: Ward's linkage distance) using the following definition as in [24]:

$$d(r,s) = \sqrt{\frac{2n_r n_s}{(n_r+n_s)}} \|\bar{x}_r - \bar{x}_s\|_2 \quad (1)$$

where n_r and n_s are the number of elements in clusters r and s, respectively, and $\bar{x}_r$ and $\bar{x}_s$ are the centroid patterns of clusters r and s, respectively. The equation was obtained from the concept of Ward's linkage, which computes the merging cost of two clusters in a hierarchical cluster method. According to previous studies [24,29], this concept can be applied to measure the distinctiveness between clusters.

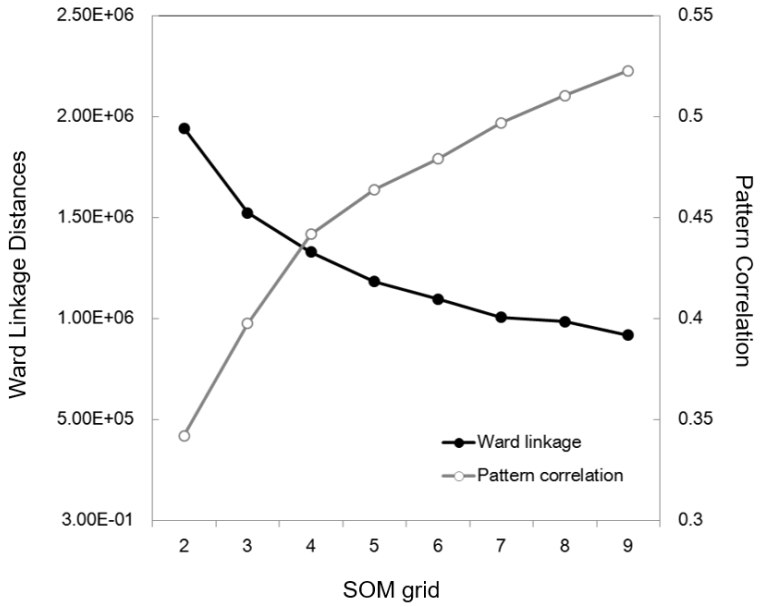

Figure 1. Ward linkage distances between SOM patterns (open circle, left y-axis), and average pattern correlations of the daily MSLP fields with their best-matching SOM pattern (closed circle, right y-axis) as a function of a single-column SOM grid.

2.3. Cyclone tracking and gridding

For detection and tracking extra-tropical cyclones, the method of [30] is used without the criteria for tropical cyclone detection. Detecting cyclone centers in the Northern Hemisphere extra-tropics (north of 30°N) comprises the following three criteria: 1) a local maximum of the 850-hPa relative vorticity larger than 2.0×10-5 s-1 within each 11×11 grid window, 2) the closest local minimum of the MSLP within a 400 km radius of the local vorticity maximum found from 1), and 3) the MSLP increase by at least 15 Pa in all directions within a 500 km distance from the local pressure minimum found by 2). Followed by detecting all cyclone centers, the tracking procedure creates the temporal movement of the detected cyclones by the technique to determine the most probable migrated position at the next time step. The procedure has three steps as follows: 1) Detected cyclone centers are picked up within the circular tracking boundary (radius: 750 km) from a cyclone center at the previous time step. 2) In case of picking up one center within the boundary, it is taken as the migrated cyclone position. If there exist multiple centers, the algorithm gives priority to the nearest center in the front semicircle towards the moving direction of the cyclone, but if not, the nearest one regardless of the direction is chosen. If no cyclones are detected within the boundary, the algorithm stops

Preprints (www.preprints.org) | NOT PEER-REVIEWED | Posted: 15 July 2019 doi:10.20944/preprints201907.0185.v1

Peer-reviewed version available at Atmosphere 2019, 10, 474; doi:10.3390/atmos10080474

tracking that cyclone. 3) Among the output data of cyclone tracks, those with lifetime shorter than 1.5 days are discarded. Then the remaining cyclone tracks are archived to the final cyclone track database.

Transforming cyclone tracks into grid-cell counts has a merit for clearly presenting the distribution of cyclone activity [31]. Due to a singularity near the pole, we construct equidistant grid-cells with 500 km by 500 km centering on the pole, rather than conventional latitude-longitude grid-cells. The gridded spatial distribution is constructed for each summer. Then the gridded data are used for yielding climatology or composite. In this study, the grid-cell cyclone frequency is shown for the spatial distribution of cyclone activity, which is defined by counting only once when a cyclone enters that grid

3. Results

3.1. SOM patterns of the summer MSLP in the Arctic

The SOM analysis is applied to the daily summer MSLP fields over the Arctic domain (north of 60°N) for the period of 1979-2017. Repeated SOM analyses are carried out with varying SOM grids from (2×1) to (10×1). As described in Section 2.2, the optimal number of SOM clusters need to be objectively determined, because distinctive atmospheric circulation patterns are the bases for comparing the features of cyclone activity among the patterns. Here we follow the selection method by Lee et al. (2017). As the number of SOM patterns increases, the mean pattern correlations (grey line) increase, while the Ward's linkage distances (black line) decrease (Figure 1). The significant test with Monte Carlo random resampling reveals that the mean pattern correlations for all SOM grids are statistically significant at the 5% level. However, the decreasing tendency of Ward's linkage distances is appreciably slower when the SOM number increases from (3×1) to (4×1). This is an indication that the (3×1) grid can be the lowest optimal number enough to yield distinct SOM patterns [24]. We therefore select the (3×1) grid as the appropriate number of SOM patterns classifying the summer atmospheric circulation in the Arctic.

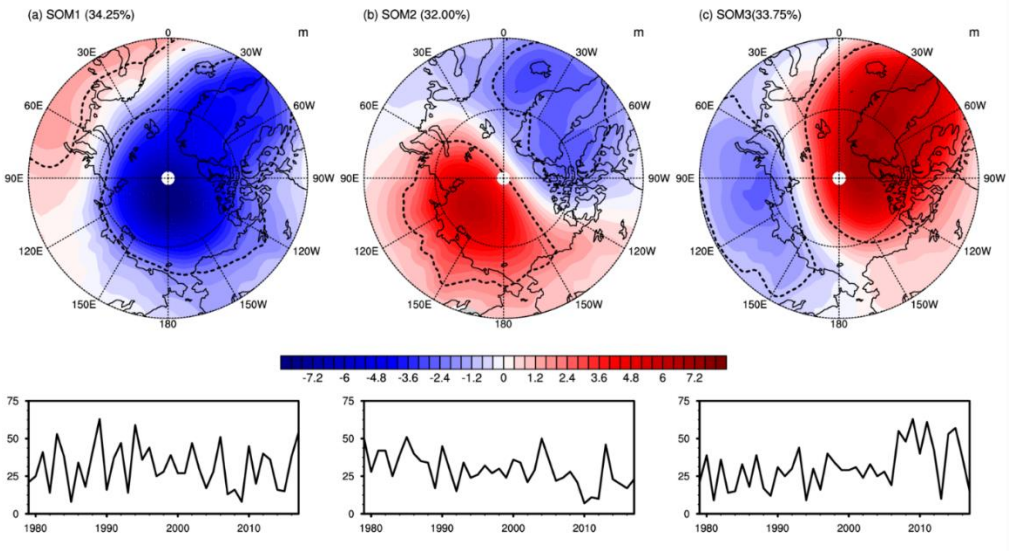

Figure 2. The SOM patterns of MSLP anomalies (hPa, top) and their time series of seasonal frequency of occurrences (day number, bottom) per summer. The percentage for each SOM indicates the occurrence frequency of that SOM pattern for 3588 days of boreal summers during 1979–-2017. The dotted lines delineate the selected core areas for yielding the cyclone activity indices used in Table 2 (SOM1: positive core ≥ 1 hPa, negative core ≤ −2 hPa, SOM2: positive core ≥ 2 hPa, negative core ≤ −2 hPa, SOM3: positive core ≥ 2 hPa, negative core ≤ −1 hPa).

Figure 2 shows spatial patterns of three SOMs (SOM1, SOM2 and SOM3) and time series of their individual occurrence frequencies for each summer (i.e., JJA). The frequency of occurrence was

obtained by counting the number of days showing the best match with a particular SOM pattern. It is found that the three SOMs almost evenly divide the summer days, indicative of three major patterns in the Arctic summer MSLP. The SOM1 shows that the negative MSLP anomaly prevails over the Arctic Ocean, except over the northern Europe, and its frequency of occurrence largely fluctuates year-to-year for the whole period (Figure 2a). The pattern resembles the polar branch of the AO during its positive phase [2, 5].

Next the SOM2 represents the dipole anomaly (DA) between the Atlantic Arctic sector and the Eurasian Arctic–Canada Basin sector (Figure 2b). Although this summertime DA of the SOM2 has a node slightly rotated counterclockwise, compared with the summertime DA of Figure 2d in [3] derived from the empirical orthogonal function (EOF) analysis, it is reasonable to say that our SOM2 DA is qualitatively similar to the negative phase of the DA of [3]. Compared with the other SOM patterns, the SOM2 has relatively lower inter-annual variability, as well as a slight decreasing trend.

By contrast, the SOM3 appears a DA-like pattern which takes on a shape opposite to the SOM2, but the node of the DA exists along the Eurasian Arctic seas (Figure 2c). It is qualitatively similar to the positive phase of the DA of [3] related with the reduction of Arctic sea-ice, which represents the anomalous anticyclonic pattern prevailing over the Canada Basin [6,9,20]. Interestingly, an abrupt increase since 2007 has been shown in the time series of the SOM3 occurrence frequency, when a large decreasing jump occurred in the time series of Arctic sea-ice extent.

The SOM-based clustered patterns in the Arctic MSLP have both similarities and discrepancies in the shape, compared with the previous EOF-based circulation patterns. The SOM analysis has advantages over the EOF analysis, in terms of its capability to yield asymmetric features and extract complex patterns [32]. Thus it is thought that the three SOM patterns reflect the real climate regimes in the summer surface atmospheric circulation of the Arctic.

3.2. Cyclone activities associated with the SOMs

Based on the three Artic surface circulation regimes (SOM1–3), here we try to identify the role of synoptic cyclone activity in forming individual circulation regimes. First, the composite maps of grid-cell cyclone frequency are constructed for the top five years with the high occurrence frequencies of individual SOMs. It is noted that the selection of years for composite uses the detrended time series. Table 1 lists the selected five years for each SOM pattern. The chosen five years for composite correspond to the top 12.5th percentile during the 39 years of 1979–2017. The results are insensitive to the number of chose years from the top four (10th percentile) to six (15th percentile) years (not shown).

Table 1. The top five years used for composite selected from the detrended time series of occurrence frequencies for each SOM.

SOM	Top five years
1	2006, 1983, 2017, 1994, 1989
2	1979, 1990. 1985, 2004, 2013
3	2015, 1980, 2007, 2011, 2009

Figure 3 presents the resultant climatological distribution of extra-tropical cyclones for the period of 1979–2017 (3a) and the composite anomalies associated with the top five years of individual SOMs (3b–d). According to [14], summer cyclones in the Arctic can be developed within the Arctic, due to enhanced thermal contrast between land and the Arctic Ocean. Consistent with their study, the activity core over the Arctic Ocean is obvious, in addition to two mid-latitude cores in the North Pacific and North Atlantic Oceans (Figure 3a).

The composite anomalies of grid-cell cyclone frequencies in the SOM1 high years show a remarkable increase over the central Arctic Ocean and Greenland–Norwegian seas (Figure 3a). Meanwhile, the cyclone frequencies in the mid-latitude North Atlantic and the Bering Sea, which are the regions where cyclone activity is climatologically frequent, tend to decrease in the SOM1 high

years. Considering the distribution of cyclone frequencies, the seasonal formation of the SOM1 pattern is closely linked to the higher synoptic cyclone activity over the central Arctic Ocean and Greenland–Norwegian seas. The MSLP anomalies associated with the SOM2 pattern are characterized by the dipole pattern between the Eurasian Arctic–Canada Basin sector and the Atlantic Arctic sector (Figure 2b). Consistent with the circulation pattern, the composite anomalies of grid-cell cyclone frequencies also show the dipole with positive anomalies around Greenland and the Canadian Arctic Archipelago and negative anomalies in the Eurasian Arctic side during the SOM2 high years (Figure 3c). During the SOM3 high years, the overall cyclone frequencies over the Arctic Ocean are significantly reduced (Figure 3d). Meanwhile, the cyclone frequencies in the mid-latitude North Atlantic and the Bering Sea increase, but those cyclones seem to seldom migrate into the Arctic Ocean. As the SOM3 pattern is the dipole dominated by the high pressure in the Arctic Ocean area (Figure 2c), it matches well with the SOM3 composite anomalies of grid-cell cyclone frequencies.

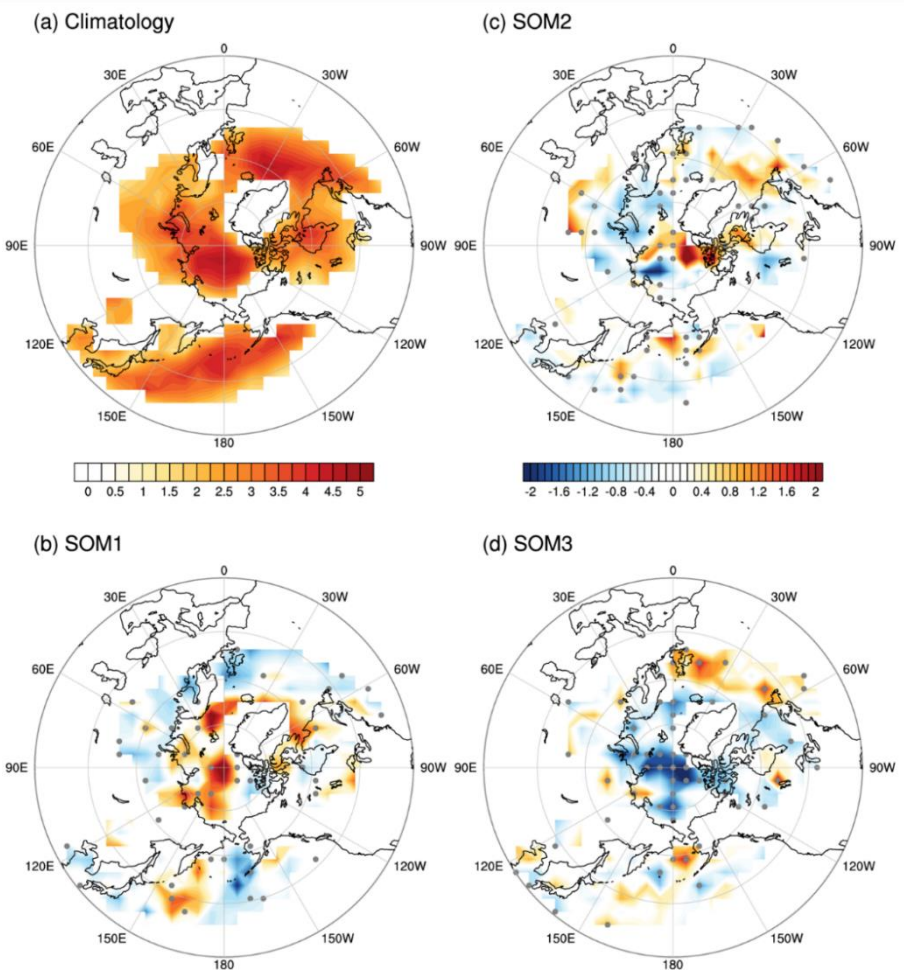

Figure 3. Climatological map of cyclone frequencies (# year^{-1}) for the period 1979–2017 (a) and their composite anomalies for the top five years selected from the detrended time series of occurrence frequencies for each SOM (b–d). The dots denote the grids where the anomaly is statistically significant at the 10% level by the Monte Carlo test.

The comparison of spatial patterns (Figure 2 vs. Figure 3) qualitatively displays the relevance of synoptic cyclone activity to the formation of summer-mean circulation patterns in the Arctic. For statistically quantifying the contribution of cyclones over the entire analysis period, the temporal correlation analysis is performed using the time series of cyclone activity indices (i.e., frequency, duration, and mean intensity) and summer-mean MSLP. The positive and negative core areas of individual SOMs are selected for constructing the time series, which are based on the anomaly

patterns in Figure 2. The frequency is constructed by counting the number of cyclones passing the core area, while the duration multiply counts all 6-hourly cyclone positions for all cyclones within the core area, then dividing the number by 4 to express in units of days. The mean intensity is defined as the average of 6-hourly central pressure data for all 6-houly cyclone positions within the core area.

Table 2. Correlation coefficients of the time series of summer-mean MSLP anomalies with three cyclone activity indices (i.e., frequency, duration and mean intensity) for the positive and negative core areas of each SOM (dotted lines in Figure 2). All the time series are obtained by averaging within individual core area. The significant correlations are denoted by one (*p*-value: 0.05) and two asterisks (*p*-value: 0.01) by the two-sided Student's t test.

SOM	Activity Core	Frequency	Duration	Intensity
1	Positive	−0.24	−0.32*	0.61**
	Negative	−0.6**	−0.72**	0.88**
2	Positive	−0.45**	−0.58**	0.75**
	Negative	−0.43**	−0.43**	0.68**
3	Positive	−0.67**	−0.70**	0.84**
	Negative	−0.24	−0.28	0.50**

The resultant correlation coefficients reveal that, among the indices, the mean intensity has the highest absolute correlations that are statistically significant at 5% level for all core areas of all SOM patterns (Table 2). This result stands to reason because the cyclone central pressure itself is the variable equivalent to the MSLP. Therefore the overall cyclone intensity is the most effective determiner of the seasonal-mean MSLP anomaly pattern in the Arctic. The duration is the second effective determiner and the frequency is the last, though in some cases (e.g., the negative core area of the SOM2, the positive core area of the SOM3) the frequency plays a significant role that is almost equivalent to the duration. Over the positive core area of the SOM1 and the negative core area of the SOM3, neither the frequency nor the duration of synoptic cyclones are effective indices for the formation of the seasonal-mean MSLP anomaly. However, these areas are not primary cores, but secondary in those SOM patterns (Figure 2).

3.3. Large-scale fields relevant to the cyclone activity forming each SOM

We have shown that the spatio-temporal variation of extra-tropical cyclones contributes significantly to the formation of the summer-mean circulation pattern in the Arctic. Now it is necessary to understand the large-scale atmospheric fields providing a background for their spatio-temporal variation. As a primary energy source of extra-tropical cyclones, the baroclinic instability is modulated by the changes in the meridional temperature gradient (the vertical shear of horizontal winds), thus we display the composite anomalies of the 200-hPa zonal wind (U200) and skin temperature (T_s) for the top five years of individual SOMs (Figure 4). As an indicator of baroclinicity, the Eady growth rate and the vertical shear of zonal winds (200 minus 850 hPa) were also investigated, but the U200 is solely shown as it primarily determines both the Eady growth rate and the vertical wind shear. In the climatological pattern, the summer T_s around the Arctic Circle shows a large gradient between land and ocean, and the higher speed of U200 appears along the mid-latitude jets (Figure 4a).

For the SOM1 high years (Figure 4a), warm T_s anomalies are distributed over the Western Europe, Ural Mountains, Northern Territories of Canada, and far-eastern Russia, while weaker cold T_s anomalies are located north of those warm T_s anomalies. This indicates the stronger meridional temperature gradient and thus forms the positive U200 anomalies (i.e., the larger vertical shear of zonal winds) north of the warm T_s anomalies. The faster U200 prevails over the Arctic Ocean rim and the northern North Atlantic Ocean, leading to more frequent poleward migration of synoptic

cyclones from the North Atlantic Ocean as well as local cyclogenesis in the Arctic. Actually, this result for the SOM1 high years can be naturally expected because the areas of the faster U200 coincide with those with climatologically frequent cyclone activity such as the northern Russian coast, Canadian Arctic Archipelago, and northern North Atlantic Ocean (Figure 3a).

Next, for the SOM2 high years (Figure 4b), there are two Arctic areas with warm T_s anomalies: one from the Barents Sea towards the Taymyr Peninsula in the far north of Russia and the other over Alaska, and also two Arctic areas with cold T_s anomalies: one over northeastern Russia and the other over the Canadian Arctic Archipelago. However, the anomalies are only statistically significant over the Barents Sea and northeastern Russia. Accordingly, the statistically significant U200 anomalies are also appreciable around those regions. Though not as clear as for the composite anomalies in the SOM1 high years, these overall U200 weakening surrounding the Eurasian Arctic could contribute to the less cyclone activity therein (Figure 3c).

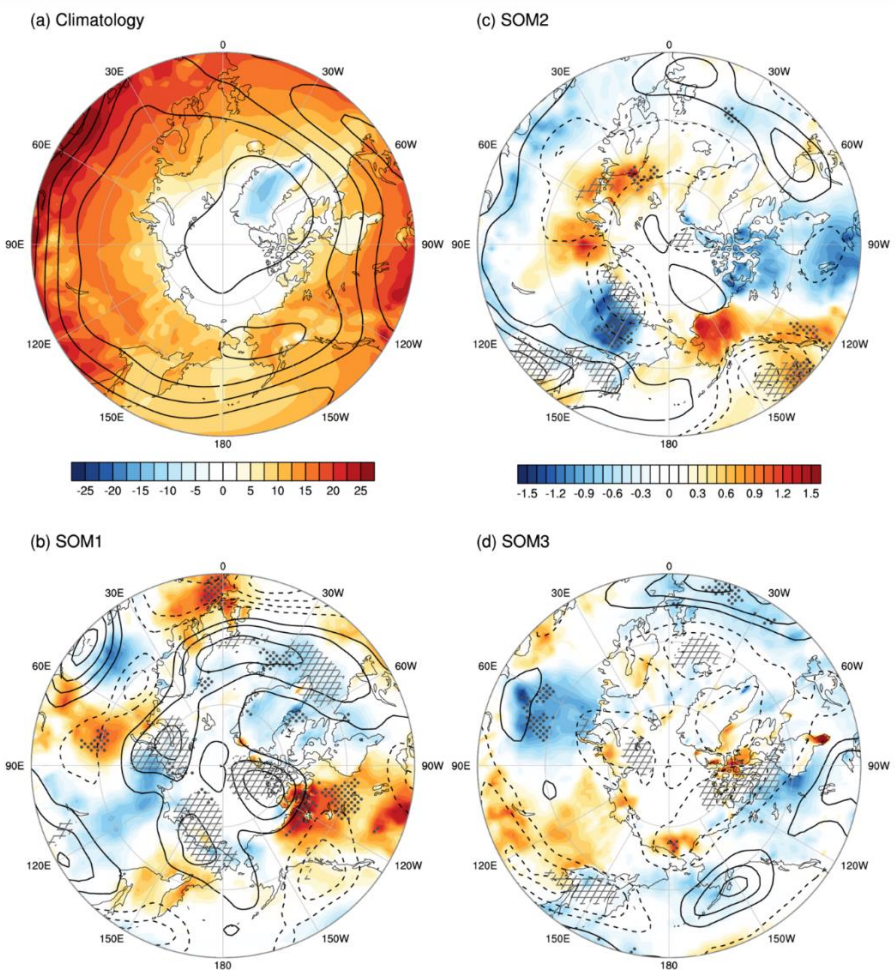

Figure 4. Same as Figure 3 except for the fields of T_s (shading, °C) and U200 (contour, m s^{-1}). The dots and hatches respectively denote the grids of T_s and U200 where their anomalies are significant at the 5% level by the two-sided Student's t test.

Lastly, composite anomalies in the SOM3 high years partly show a state opposite to those in the SOM1 high years (Figure 4c). This means the reduced meridional temperature gradient and slower U200 surrounding the Arctic Ocean rim and the northern North Atlantic Ocean, resulting in less cyclone migration from the North Atlantic Ocean as well as overall reduced cyclogenesis in the Arctic (Figure 3d).

3.4. Synoptic evolution associated with the SOMs

Given the significant role of synoptic cyclones in the formation of summer-mean Arctic circulation patterns as clustered by the SOMs, it would be informative to characterize the generalized daily evolution of synoptic activity for each SOM by constructing lead-lag composites based on the central days (i.e., lag day 0) of each SOM. The central days of a certain SOM are the best-matching days with the SOM pattern (Figure 2). Here consecutive days with the same SOM pattern is defined as a single event of that SOM. If there are two or more days of one SOM event, the best-matching day is selected among the days that has the smallest root mean square error (RMSE) between the daily MSLP anomaly pattern and the SOM pattern. Through this searching process, we identify 109 events of the SOM1, 112 of the SOM2, and 114 of the SOM3, respectively, for the period of 1979–2017. Prior to constructing lead-lag composites, 15-day moving averages are subtracted from the daily data in order to focus only on the synoptic-scale variability. In Figures 5–7, the daily evolutions for individual SOMs are shown with the 500-hPa geopotential height (H500).

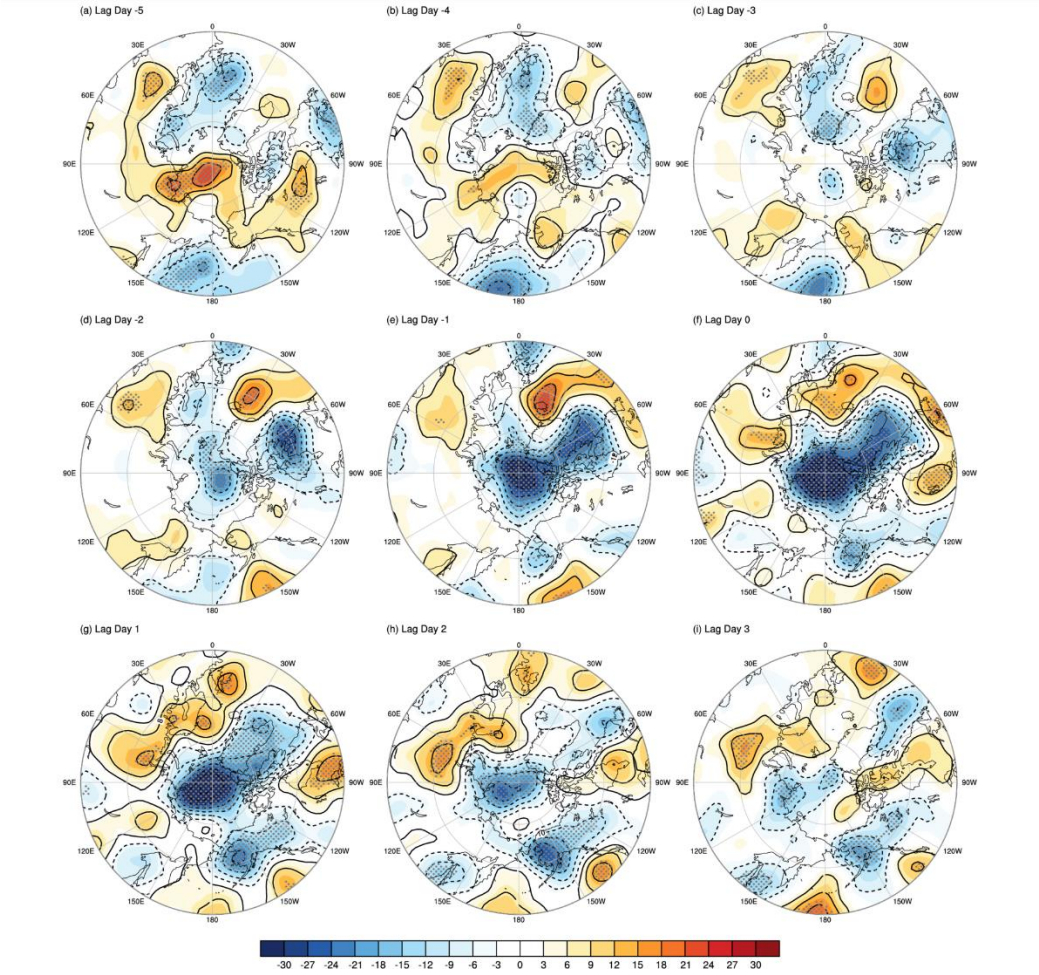

Figure 5. Composite daily evolutions of the synoptic-scale H500 anomalies (gpm) from −5 to +3 days for the 109 best-matching events of the SOM1. The dots denotes the grids where the anomalies are statistically significant at the 5% level by the two-sided Student's t-test.

The composite daily evolution associated with the 109 SOM1 events (Figure 5) shows as to how the prevailing low pressure system takes up the entire Arctic Ocean at lag day 0 (Figure 5f). From lag day −5 to −2 (Figure 5a–c), the northward migrating low pressure composite is detected in the Norwegian Sea and the East Siberian Sea, where only the former is statistically significant at the 5% level. They quickly erase the preexisting high pressure composite in the Central Arctic Ocean and get stronger until lag day 0. Meanwhile, another low pressure composite develops around Quebec, Canada and extends northward. Eventually a massive low pressure composite occupies the Arctic

Ocean towards Greenland (Figure 5f). The low pressure composite in the Arctic Ocean is sustained significantly until lag day 2 (Figure 5h) and then weakens at lag day 3 (Figure 5i).

Figure 6 shows the composite daily evolution for the 112 best-matching events of the SOM2. At lag day −5, a reversed dipole analogous to the SOM3 pattern exists (Figure 6a). This pattern is quickly transformed to the incipient stage of the SOM2 during lag day −4 to −3 by the developing high pressure composite over the Taymyr Peninsula and Laptev Sea and the developing low pressure composite in-and-around Greenland (Figure 6b–c). These two opposite pressure systems further develop and then the SOM2-like dipole pattern prevails in the Arctic from lag day −2 to lag day 1 (Figure 6d–g). After the SOM2 event, the low pressure system tends to prevail over the Arctic Ocean (Figure 6h–i). Based on the composite evolutions, the SOM2 event seems to last shorter than the SOM1 event.

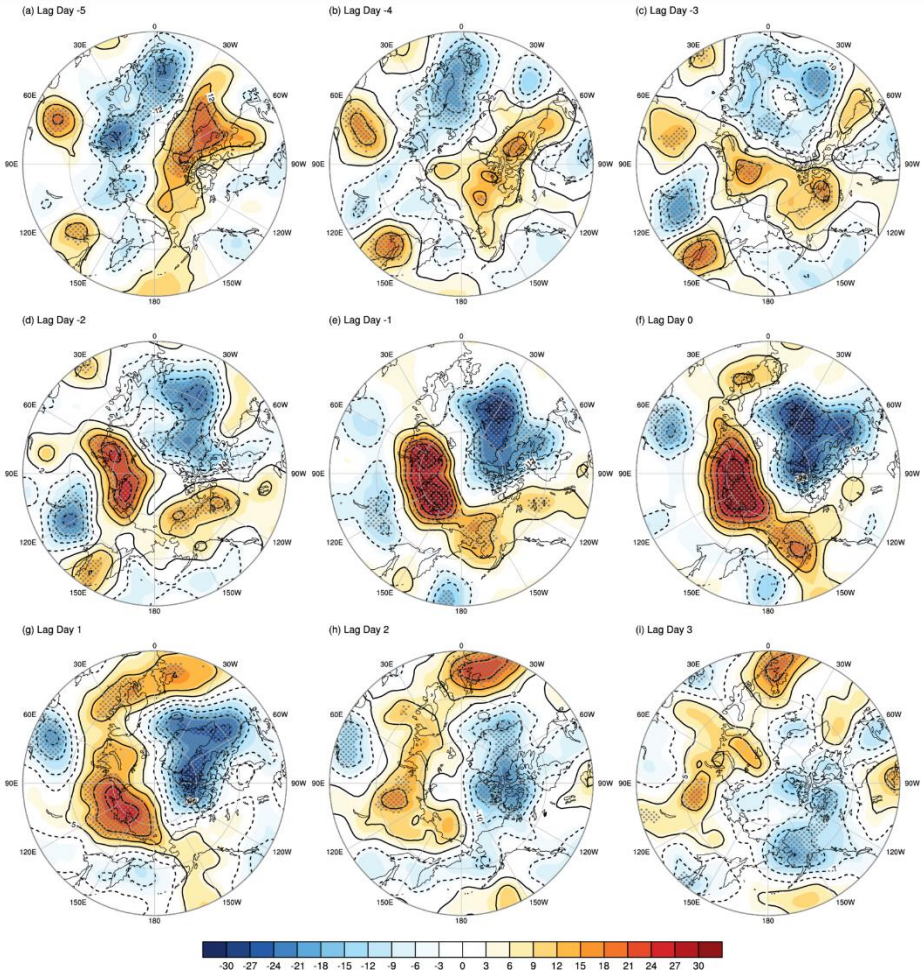

Figure 6. Same as Figure 5 except for the 112 best-matching events of the SOM2.

Lastly, the composite daily evolution is presented in Figure 7 for the 114 best-matching events of the SOM3. Similar to the SOM2, there exist a dipole opposite to the SOM3 pattern at lag day −5 (Figure 7a). The high pressure composite around the Barents–Kara seas are pronounced, but it weakens in three days (Figure 7b–d). The low pressure composite gradually develops and replaces the high in the far north of Russia around the Kara–Laptev seas (Figure 7d–f), while the high pressure composite begins to develop in the Beaufort Sea and then expands towards the central Arctic Ocean (Figure 7b–f). The SOM3 event shows persistence after the peak day until lag day 3 (Figure 7g–i).

Preprints (www.preprints.org) | NOT PEER-REVIEWED | Posted: 15 July 2019 doi:10.20944/preprints201907.0185.v1

Peer-reviewed version available at Atmosphere 2019, 10, 474; doi:10.3390/atmos10080474

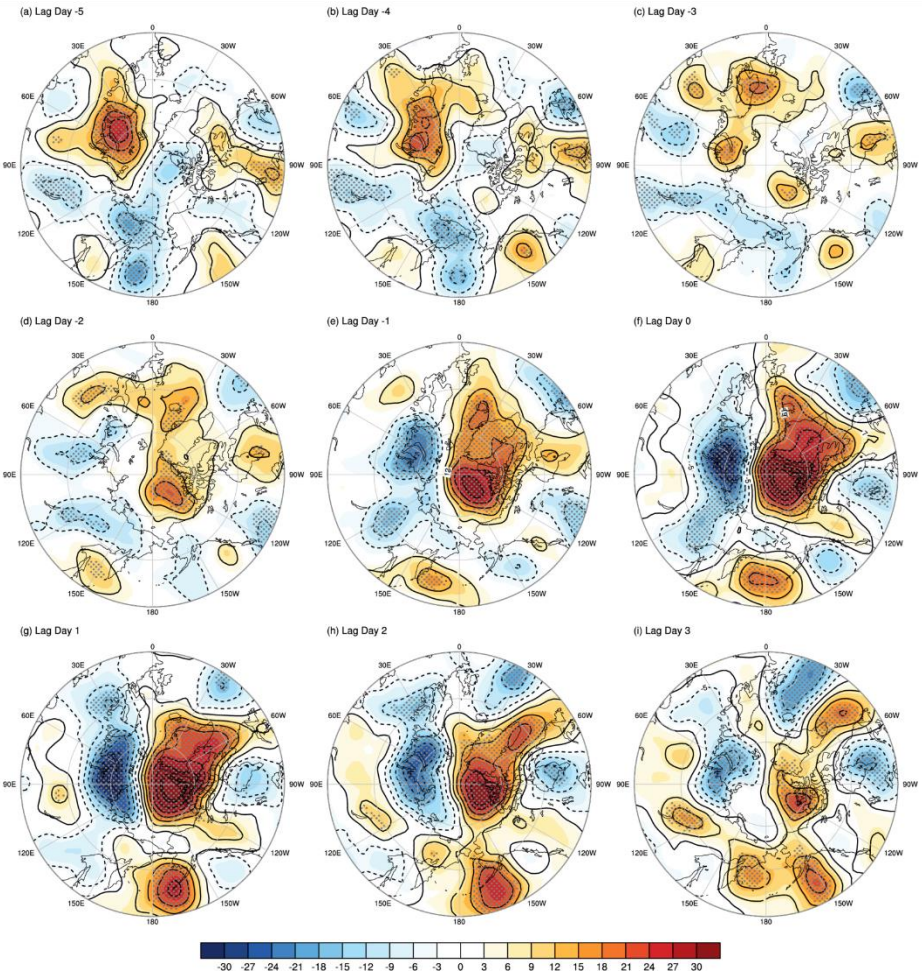

Figure 7. Same as Figure 5 except for the 114 best-matching events of the SOM3.

4. Summary and Discussion

The formation of monthly-to-seasonal atmospheric circulation patterns by low-frequency modes in the Arctic has been extensively studied in terms of their influences on Arctic climate and sea ice [1–9]. Researches have also shown that the activity of synoptic cyclones is more prevalent during summer in the Arctic Ocean [13–15] and suggested their potential contribution to seasonal-mean Arctic climate [13,14,20]. Our results further added the quantitative contribution of synoptic cyclone activity to the amplitude of the seasonal-mean anomalies in the individual activity cores of three dominant Arctic summer circulation patterns as clustered by the SOM method (Table 1), and also confirm that the spatio-temporal distribution of synoptic cyclones in the Arctic domain is a major controlling factor for the Arctic summer circulation patterns (Figures 2–3). Furthermore, the summer cyclone activity in the central Arctic Ocean is enhanced only for the circulation pattern (e.g., SOM1) that the land–Arctic Ocean boundary area with enhanced baroclinicity (i.e., the increased meridional temperature gradient) is co-located with the climatological major cyclone pathways (Figures 3–4).

The composite daily synoptic evolutions well demonstrated the generalized formation processes and the timescales of the three SOM patterns of the atmospheric circulation in the Arctic (Figures 5–7). Although their evolutions have been shown with the high-pass filtered data by retaining only the synoptic-scale variability, it is naturally expected to be almost consistent with those obtained from the unfiltered daily data. The reason for this expectation is because the evolutionary SOM patterns as shown in Figures 5–7 have just a couple of days timescale (i.e., within the synoptic-scale variability), with e-folding times of 4.4, 3.6 and 3.6 days for the SOM1–3, respectively. According to previous literature, these short timescale weather evolutions have substantial variability at inter-annual and longer timescales beyond the climate noise [32– 34]. Therefore, it is reasonable to contend that the

summer-mean Arctic circulation patterns reflect the accumulation of short timescale events, such as synoptic cyclones here or anticyclones as studied by [20].

The Arctic is not an isolated region but retains the Norther Hemispheric high-latitude components of the global climate system that actively interact with lower latitudes [36–38]. Therefore, the inter-annual and longer-timescale changes in the Arctic circulation patterns should be understood in the context of global climate variability. Further studies are necessary to investigate as to which type of climate variability over the globe provides a relevant teleconnection for the different summer climatic states in the Arctic.

Author Contributions: Individual authors contributions are summarized as follows: "conceptualization, J.-H.K.; methodology, M.-H.L.; formal analysis, M.-H.L.; writing—original draft preparation, M.-H.L. and J.-H.K.; writing—review and editing, J.-H.K.; visualization, M.-H.L.; supervision, J.-H.K.; project administration, J.-H.K.; funding acquisition, J.-H.K."

Funding: This study was funded by the Korea Polar Research Institute (KOPRI) project, entitled 'Development and Application of the Korea Polar Prediction System (KPOPS) for Climate Change and Weather Disasters' (KOPRI, PE19130).

Acknowledgments:

Conflicts of Interest: The authors declare no conflict of interest

References

1. Rigor, I.G.; Wallace, J.M.; Colony, R.L. Response of sea-ice to the Arctic Oscillation. *J. Clim*. **2002**, *15*, 2648–2663, doi: 10.1175/1520-0442(2002)015<2648:ROSITT>2.0.CO;2.
2. Rigor, I.G.; Wallace J.M. Variations in the age of Arctic sea-ice and summer sea-ice extent, *Geophys. Res. Lett*. **2004**, *31*, L09401, doi: 10.1029/2004GL019492.
3. Wang, J.; Zhang, J.; Watanabe, E., Ikeda, M.; Mizobata, K.; Walsh, J.E.; Bai X.; Wu B. Is the Dipole Anomaly a major driver to record lows in Arctic Summer sea ice extent? Geophys. Res. Lett. **2009**, *35*, L05706, doi: 10.1029/2008GL036706.
4. Ogi, M.; Wallace, J.M. Summer minimum Arctic sea ice extent and the associated summer atmospheric circulation. *Geophys. Res. Lett*. **2007**, *109*, D20114, doi: 10.1029/2004JD004514.
5. Ogi, M.; Yamazaki, K. Trends in the summer northern annular mode and Arctic sea ice. *SOLA* **2010**, *6*, 41–44, doi: 10.2151/sola.2010-011.
6. Ogi, M.; Wallace, J.M. The role of summer surface wind anomalies in the summer Arctic sea ice extent in 2010 and 2011. *Geophys. Res. Lett*. **2012**, *39*, L09704, doi: 10.1029/2012GL051330.
7. Screen, J.A.; Simmonds, I.; Keay, K. Dramatic interannual changes of perennial Arctic sea ice linked to abnormal summer storm activity. *J. Geophys. Res*. **2011**, *116*, D15105, doi: 10.1029/2011JD015847.
8. Knudsen, E. M.; Orsolini Y.J.; Furevik, T.; Hodges K.I. Observed anomalous atmospheric patterns in summers of unusual Arctic sea ice melt. *J. Geophys. Res*. **2015**, *120*, 2595–2611, doi: 10.1002/2014JD022608.
9. Ding, Q.; Co-authors. Influence of high-latitude atmospheric circulation changes on summertime Arctic sea ice. *Nat. Clim. Chang*. **2017**, *7*, 289–295, doi: 10.1038/nclimate3241.
10. Kapsch, M.; Graversen R.G.; Tjernström M. Springtime atmospheric energy transport and the control of Arctic summer sea–ice extent. *Nat. Clim. Chang*. **2013**, *3*, 744–748, doi: 10.1038/nclimate1884.
11. Park, H.-S.; Lee, S.; Kosaka, Y.; Son, S.-W.; Kim, S.-W. The impact of Arctic winter infrared radiation on early summer sea ice. *J. Clim*. **2015**, *28*, 6281–6296, doi: 0.1175/JCLI-D-14-00773.1.
12. Williams, J.; Tremblay, B.; Newton, R.; Allard, R. Dynamic preconditioning of the minimum September sea-ice extent. *J. Clim*. **2016**, *29*, 5879–5891, doi: 10.1175/JCLI-D-15-0515.1.
13. Zhang X; Walsh, J. E.; Zhang, J.; Bhatt, U.S.; Ikeda, M. Climatology and interannual variability of Arctic cyclone activity: 1948–2002. *J. Clim*. **2004**, *17*, 2300–2317, doi: 10.1175/1520-0442(2004)017<2300:CAIVOA>2.0CO;2.
14. Serreze. M.C.; Barrett. A.P. The summer cyclone maximum over the central Arctic Ocean. *J. Clim*. **2008**, 21, 1048–1065, doi: 10.1175/2007JCLI1810.1.

15. Orsolini, Y.J.; Sorteberg, A. Projected changes in Eurasian and Arctic summer cyclones under global warming in the Bergen Climate Model. *Atmos. Oceanic Sci. Lett.* **2009**, *2*, 62–67, doi: 10.1080/16742834.2009.11446776.
16. Crawford, A.D.; Serreze, M.C. A new look at the summer Arctic frontal zone. *J. Clim.* **2015**, *28*, 737–754, doi: 10.1175/JCLI-D-14-00447.1.
17. Mesquita, M.; Kvamstø, N.G.; Sorteberg, A.; Atkinson, D.E. Climatological properties of summertime extra-tropical storm track in the Northern Hemisphere. *Tellus A.* **2008**, *60*, 557–569, doi: 10.1111/j.1600-0820.2008.00305.x.
18. Simmonds, I. Rudeva, I. The great Arctic cyclone of August 2012. *Geophys. Res. Lett.* **2012**, *39*, L23709, doi: 10.1029/2012GL054259.
19. Semenov, A.; Zhang, X.; Rinke, A.; Dorn, W.; Dethloff, K. Arctic intense summer storms and their impacts on sea ice – a regional climate modeling study. *Atmos.* **2019**, *10*, 218, doi: 10.3390/atmos10040218.
20. Wernli, H.; Papritz, L. Role of polar anticyclones and mid-latitude cyclones for Arctic summertime sea-ice melting. *Nat. Geosci.* **2018**, *11*, 108–113, doi: 10.1038s41561-017-0041-0.
21. Johnson, N.C. How many ENSO flavors can we distinguish? *J. Clim.* **2013**, *26*, 4816–4827, doi: 10.1175/JCLI0D012099649.1.
22. Lee, S.; Feldstein, S.B. Detecting ozone- and greenhouse gas-driven wind trends with observational data. *Science* **2013**, *339*, 563–567, doi: 10.1126/sciences.1225154.
23. Bao, M.; Wallace, J.M. Cluster analysis of Northern Hemisphere wintertime 500-hPa flow regimes during 1920–2014. *J. Atmos. Sci.* **2015**, *72*, 3597–3608, doi: 10.1175/JAS-D-15-0001.1.
24. Lee, M.-H.; Lee, S.; Song, H.-J.; Ho, C.-H. The recent increase in the occurrence of a boreal summer teleconnection and its relationship with temperature extremes. *J. Clim.* **2017**, *30*, 7493–7504, doi: 10.1175/JCLI-D-16-0094.1.
25. Dee, D.P.; Co-authors. The ERA-Interim reanalysis: Configuration and performance of the data assimilation system. *Quart. J. Roy. Meteor. Soc.* **2011**, *137*, 553–597, doi: 10.1002/qj.828.
26. Johnson. N.C; Feldstein, S.B.; Tremblay, B. The continuum of Northern Hemisphere teleconnection patterns and a description of the NAO shift with the use of self-organizing maps. *J. Clim.* **2008**, *21*, 6354–6371, doi: 10.1175/20089JCLI2380.1.
27. Kohonen, T. Self-Organizng Maps, 3rd ed.; *Springer* **2001**; 521pp.
28. Leloup, J.; Lachkar, Z.; Boulaner, J.-P.; Thiria, S. Detecting decadal changes in ENSO using neural networks. *Clim. Dyn.* **2007**, *28*, 147–162, doi: 10.1007/s00382-006-0173-1.
29. Xu, G.; Zong, Y.; Yang, Z. Applied Data Mining.; *CRC Press* **2013**; 284pp.
30. Vitart, F.; Anderson, J.L.; Stern, W.F. Simulation of interannual variability of tropical storm frequency in an ensemble of GCM integrations. *J. Clim.* **1997**, *10*, 745–760 doi: 10.1175/1520-0442(1997)010<0745:SOIVOT>2.0.CO;2.
31. Liu, Y.; Weisberg R.H. A review of self-organizing map applications in meteorology and oceanography. In Self-Organizing Map- Applications and Novel Algorithm Design.; Mwasiagi, J.I., Ed.; InTech: Rijeka, Croatia, 2011, pp. 253–272.
32. Leith, C.E. The standard error of time-averaged estimates of climatic means. *J. Appl. Meteor.* **1973**, *12*, 1066–1069, doi: 10.1175/1520-0450(1973)012,1066:TSEOTA.2.0.CO;2.
33. Madden, R.A. Estimates of the natural variability of time averaged sea-level pressure. *Mon. Wea. Rev.* **1976**, 104, 942–952, doi: 10.1175/1520-0493(1976)104,0942:EOTNVO.2.0.CO;2.
34. Feldstein, S.B. Teleconnections and ENSO: The timescales, power spectra, and climate noise properties. *J. Clim.* **2000**, *13*, 4430–4440, doi: 10.1175/1520-0442(2000)013,4430:TTPSAC.2.0.CO;2.
35. Cohen, J.; Screen, J. A.; Furtado, J. C.; Barlow, M.; Whittleston, D.; Coumou, D.; Francis, J.; Dethloff, K.; Entekhabi, D.; Overland, J.; Jones, J. Recent Arctic amplification and extreme mid-latitude weather. *Nat. Geosci.* **2014**, 7, 627637, doi: 10.1038/s41467-018-05256-8.
36. Overland, J.; Francis, J.A.; Hall, R.; Hanna, E.; Kim, S.-J.; Vihma, T. The melting Arctic and midlatitude weather pattern: Are they connected? *J. Clim.* **2015**, *28*, 7917–7932, doi: 10.1175/JCLI-D-14-00822.1.
37. Coumou, D.; Capua, G.D.; Vavrus, S.; Wang, L.; Wang, S. The influence of Arctic amplification on mid-latitude summer circulation. *Nat. Commun.* **2018**, *9*, 2959, doi: 10.1038/s41467-018-05256-8.